Improving Seasonal Predictions of Climate Variability and Water Availability at the Catchment Scale

MATTHEW B. SWITANEK AND PETER A. TROCH

Department of Hydrology and Water Resources, The University of Arizona, Tucson, Arizona

CHRISTOPHER L. CASTRO

Department of Atmospheric Sciences, The University of Arizona, Tucson, Arizona

(Manuscript received 9 July 2008, in final form 22 May 2009)

ABSTRACT

In a water-stressed region, such as the southwestern United States, it is essential to improve current seasonal hydroclimatic predictions. Typically, seasonal hydroclimatic predictions have been conditioned by standard climate indices, for example, Niño-3 and Pacific decadal oscillation (PDO). In this work, the statistically unique relationships between sea surface temperatures (SSTs) and particular basins' hydroclimates are explored. The regions where global SSTs are most correlated with the Little Colorado River and Gunnison River basins' hydroclimates are located throughout the year and at varying time lags. The SSTs, from these regions of highest correlation, are subsequently used as hydroclimatic predictors for the two basins. This methodology, named basin-specific climate prediction (BSCP), is further used to perform hindcasts. The hydroclimatic hindcasts obtained using BSCP are shown to be closer to the historical record, for both basins, than using the standard climate indices as predictors.

1. Introduction

Lake Powell divides the upper and lower Colorado River basins and has historically had sufficient storage to provide both regions with the quantities of water set by the Colorado River Compact. The current drought, which began in 2000, however, has shown that Lake Powell's storage is susceptible to natural climate variability and cannot always be relied upon. In April 2005, Lake Powell's storage was 33% of live capacity because of yearly inflows that were, on average, approximately 59% below normal. Rising temperatures across the southwestern United States, associated with global climate change, could further exacerbate droughts in the Colorado River basin (Barnett et al. 2005, 2008; McCabe and Wolock 2007; Hoerling and Eischeid 2007). The projected temperature increase and accompanying increase in evapotranspiration are anticipated to decrease runoff in the Colorado River basin between 6%–30% over the next 50 years (Milly et al. 2005; Christensen et al. 2004; Christensen and Lettenmaier 2007). Since the signing of the Colorado River Compact in 1922, the demand for water to be used for municipality, agriculture, and hydropower has grown rapidly. In addition to this increase in demand, climate projections are expected to decrease supply and further stress the water resources in the Colorado River basin. To aid decision makers and stakeholders in the allocation of this stressed resource in the Southwest, it is essential to improve hydroclimatic seasonal predictions.

Most of the variability in Lake Mead's pool elevation is governed by releases from Lake Powell. In the event that a drought restricts Lake Powell's releases to an amount less than required by the Colorado River Compact, tributaries between Powell and Mead will play a significant role in the Lower Colorado basin states' water supply. Therefore, development and improvement of hydroclimatic predictions needs to take place at the subbasin scale (e.g., Little Colorado River basin or Paria River basin). Improving these subbasin predictions can provide a more detailed map of water availability for the entire Colorado River basin, thus reducing potential uncertainty confronting water managers.

Corresponding author address: M. B. Switanek, Department of Hydrology and Water Resources, The University of Arizona, 1133 E. James E. Rogers Way, Rm. 320A, Tucson, AZ 85721.
E-mail: mbswitan@email.arizona.edu

DOI: 10.1175/2009JHM1073.1

© 2009 American Meteorological Society

The earth's oceans have a vast storage of energy that helps drive global climatic variability. Sea surface temperatures (SSTs) are one manifestation of this energy storage. Given the oceanic mass and water's large specific heat, SSTs' effect on ocean–atmosphere heat and water vapor exchange can be on seasonal to annual time scales. Consequently, variability in SSTs can help provide predictive information about the hydroclimate in regions across the globe. Over the past several decades, the statistical link between regional SST variability [e.g., the El Niño–Southern Oscillation (ENSO), the Pacific decadal oscillation (PDO) and the Atlantic multidecadal oscillation (AMO)] and global surface hydroclimatic variability has been well established (Trenberth 1997; Namias and Cayan 1984; Redmond and Koch 1991; Ropelewski and Halpert 1996; Enfield et al. 2001). Niño-3 is a commonly used index of ENSO, in which Niño-3 is the area average of the SSTs over the domain between 5°N and 5°S latitude and between 210° and 270°E longitude (east of the prime meridian). The PDO index is calculated to be the first principal component [derived from a principal component analysis (PCA)] of detrended SST anomalies northward of 20°N latitude in the Pacific Ocean (Mantua et al. 1997), whereas the AMO is essentially the detrended, area-weighted average of SSTs over the North Atlantic Ocean.

At seasonal to interannual time scales, there are numerous studies documenting the statistical connectivity of ENSO to land surface variables affecting hydroclimatic variability, including temperature (Higgins et al. 2000), precipitation (Ropelewski and Halpert 1996; McCabe and Dettinger 1999; Kim et al. 2005), and streamflow (Piechota et al. 1997; Cayan et al. 1999; Gochis et al. 2007). McCabe and Dettinger (1999) correlate Niño-3 with western U.S. precipitation and show statistically significant regions (these regions have correlation coefficients that are not a result of chance, at the 95% confidence interval). They, in addition to other studies, observe a negative correlation between Niño-3 and winter precipitation in the Northwest, whereas Niño-3 and winter precipitation in the Southwest exhibit a positive correlation.

Forecasts of precipitation and temperature, made by the Climate Prediction Center (CPC), are typically used by the River Forecast Centers to force statistical and hydrological models to simulate naturalized streamflows across the western United States. The CPC currently uses the present state of ENSO to condition these seasonal climatic forecasts. There are two potential problems with using standard climate indices—such as Niño-3, PDO, and AMO—for hydroclimatic prediction. The first problem is that the hydroclimate of a specific terrestrial region (e.g., a river basin) may be more strongly correlated with an oceanic region's SSTs, which is different from the predetermined regions that are used to calculate the standard indices. Historically, there have been numerous studies that have documented broad-scale ocean–atmosphere teleconnections that are not directly tied to standard climate indices (Namias 1969, 1974, 1978; Kutzbach 1970; Nicholls 1980). More recently, Tootle and Piechota (2006) use SSTs for an entire region, such as the Pacific Ocean. They use singular value decomposition (SVD) to identify and delineate statistically significant, covarying regions between U.S. streamflow and Pacific SSTs. The second problem with some of the standard indices is that a matrix methods approach (e.g., PCA and SVD) might not preserve enough information from an original dataset. Some recent hydroclimatic studies—such as Dettinger and Cayan (1995), Rucong et al. (2001) and Grantz et al. (2005)—have abandoned a matrix methods approach.

The study herein extends the Grantz et al. (2005) methodology in the following ways. First, Grantz et al. (2005) only use streamflow in their analysis, whereas we also use precipitation and temperature. Given the level of human influence along most of the rivers in the western United States, it is important to have climatic values to force a hydrological model, thereby obtaining an expected naturalized volume of water. A natural streamflow time series needs to be long enough in the past to calibrate the model. However, if model calibration is possible, then precipitation and temperature offer another way to independently obtain expected water availability for a particular basin. Second, they try to establish unique correlative relationships and potential predictors exclusively for spring discharge at lead times of up to six months. We include all trimonthly seasons through the entire year and are developing potential predictors for these seasons at up to a year ahead of time. Third, Grantz et al. (2005) use SSTs for predicting spring discharge at six and five months' lead time but then condition the predictions with snow water equivalent (SWE) data. We are aware that a snow-dominated system's spring snowmelt will be very strongly influenced by winter SWE; however, we chose to explore the raw potential of using solely SSTs as predictors. We are providing one of the components that assists in constraining expected seasonal hydroclimatic distributions. Lastly, we use the entire oceanic domain, whereas Grantz et al. (2005) observe the correlative structures mostly in the Pacific and the western Atlantic Oceans.

The objective of this study is to outline a methodology that has the capacity to improve current basin-specific hydroclimatic predictions at the seasonal to annual time scale. The section ''Materials'' describes the Little Colorado River and Gunnison River basins and the data

used in the study. The section ''Methodology'' outlines the basin-specific climate prediction (BSCP) approach. The precipitation, temperature, and streamflow data from the Little Colorado and the Gunnison are correlated with global SSTs. The statistical correlative oceanic patterns, using BSCP, are observed at different months of the year and at different time lags. Using these statistical patterns, the SSTs from the regions that exhibit the strongest correlation are subsequently used as predictors to perform hindcasts of each basin's hydroclimate. Niño-3, Niño-3.4 (5°N–5°S, 190°–240°E), Multivariate ENSO index (MEI), and PDO are also used as predictors to perform hindcasts. The section ''Results'' compares the hindcast skill of BSCP to the standard climate indices. The section ''Discussion and conclusions'' highlights the results and concludes with a few recommendations for further research on seasonal hydroclimatic prediction.

2. Materials

a. Regions of study

The Little Colorado River is located in the Lower Colorado River basin and comprises approximately 68 500 km^2. The basin's elevation ranges between 3850 m in the San Francisco peaks to approximately 840 m at the outlet. The Little Colorado receives as little as 36 mm of average seasonal total precipitation during the April–June season and as much as 127 mm for July–September. Average seasonal temperatures historically have ranged between 0.3°C for the December–February season and 20.8°C for June–August. Streamflow for the Little Colorado River originates in eastern Arizona and flows northwest for almost 507 km until meeting the Colorado River in the Grand Canyon (Fig. 1). The average yearly streamflow volume totals approximately 220×10^6 m^3, with average seasonal rates being highly variable between 80 m^3 s^{-1} to essentially no flow.

The Gunnison River is located in the upper Colorado River basin and is approximately 20 800 km^2. The basin's elevation ranges between 4400 to approximately 1390 m at its junction with the Colorado River. The Gunnison average seasonal total precipitation ranges between 115 mm during the June–August season and 160 mm for February–April. Average seasonal temperatures historically have ranged between −9.2°C for the December–February season and 13.8°C for June–August. Streamflow originates in the Rocky Mountains and flows west–northwest for almost 290 km until meeting the Colorado River. The average yearly streamflow volume totals approximately 2.76×10^9 m^3, with average seasonal rates ranging between 215 and 38 m^3 s^{-1}.

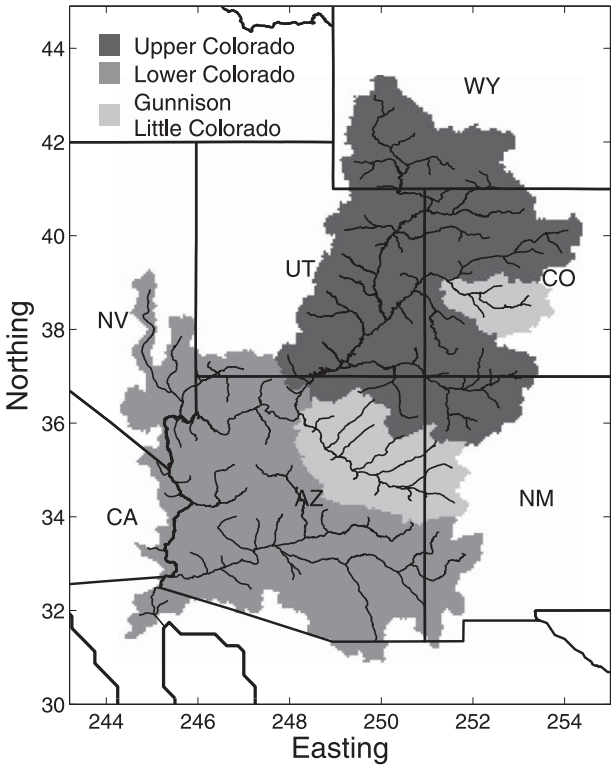

FIG. 1. The Gunnison River basin shown in light gray in the state of Colorado. The Little Colorado River basin is also shown in light gray and residing in Arizona and New Mexico.

b. Data

The precipitation and temperature data for the Little Colorado and Gunnison are obtained from an interpolated, gridded dataset (Maurer et al. 2002). The dataset was created as inputs to force the Variable Infiltration Capacity (VIC) hydrological model and provides data at a 3-h time step with a spatial resolution of $\frac{1}{8}° \times \frac{1}{8}°$. The dataset covers the conterminous United States, and this study uses the years 1951–2005. Naturalized volumetric discharge data for the basins were obtained from the Bureau of Reclamation (available online at http://www.usbr.gov/lc/region/g4000/NaturalFlow/index.html). The discharge data are provided at a monthly time step and are used for the same overlapping 55 years as the temperature and precipitation data, and the streamflows are assumed to reflect the contribution of the whole basin.

Mean monthly SSTs were obtained from the International Comprehensive Ocean–Atmosphere Data Set (ICOADS) through the University Corporation for Atmospheric Research site (available online at http://dss.ucar.edu/). The resolution of the SST data is $2° \times 2°$, and the entire oceanic domain is used. To have the same temporal domain for all of the data, the SSTs corresponding to 1951–2005 are used.

c. Data preparation

To effectively and efficiently ascertain a seasonal quantitative prediction for the Little Colorado and Gunnison basins, seasonal values for precipitation, temperature, and discharge at the basin scale are required. First, spatial averages are calculated. For discharge, it is simply a matter of dividing the volume of water for a given month by the area of the basin. For precipitation and temperature, a file containing the fractional contributions of each 1/8° grid cell is used, where the boundary of the basin is not delineated at the gridcell size but rather more accurate digital elevation maps [30-m resolution obtained through the U.S. Geological Survey (USGS) site (available online at http://seamless.usgs.gov/)], thus only fractional amounts of the bordering grid cells will contribute. By performing a weighted spatial average, the climatic values are not affected by fractions of grid cells that drain out of the basin. Each variable's weighted averages are obtained for their respective time steps. Second, average seasonal temperatures and seasonal totals of precipitation and discharge are obtained. Seasonal hydroclimate variables are averaged or integrated values at a trimonthly resolution. There are 12 trimonthly seasons, corresponding to January–March, February–April continuing through December–February. This yields the total seasonal sums of precipitation and discharge, averaged across the basin, and the seasonal averages of temperature.

In the southwestern United States, seasonal temperature generally exhibits a normal (Gaussian) distribution, whereas seasonal precipitation and discharge exhibit skewness that corresponds well with a gamma distribution. The z values, or z scores, for seasonal temperatures are computed by subtracting the population mean and dividing by the standard deviation. The standardized precipitation index (SPI) has previously been used to convert precipitation, which exhibits a gamma distribution, to normally distributed data (McKee et al. 1993; Kim et al. 2005). We convert cumulative densities from the gamma distribution to SPI values by means of an approximation provided by Abramovitz and Stegun (1972). The same SPI algorithm is applied to obtain z scores of discharge. There are two reasons why we choose to normalize precipitation and discharge. First, this allows a more accurate climate regime comparison between two different basins. Second, our methodology later requires Gaussian distributed data.

As a way to decrease the sparseness of the global SSTs, and to have a second level of quality control, the SSTs were spatially averaged on 10° × 20° latitude by longitude moving windows. As a result, we have more densely populated SSTs across the Pacific, at a 2° × 2° resolution, where each grid cell corresponds to a larger 10° latitude by 20° longitude window. Though we are advocating using SST windows that are not fixed like the Niño-3 domain, we want some consistency with the climate indices. As previously stated, the Niño-3 index is a regional SST average between 5°N and 5°S and between 210° and 270°E. Indices like Niño-3 are using anomalies in regions greater than the gridcell size (2° × 2°) to help describe ocean–atmosphere phenomena. Using a larger sample size in space, we can be more confident that the regional variance is more accurately depicted, thus reducing the randomness associated with individual grid cells.

3. Methodology

a. SST–basins' climate and discharge correlation maps

Using SSTs as a predictor of the climate and discharge in the Little Colorado and Gunnison, we observe the spatial correlative structure between global SSTs and seasonal basin variables at different temporal lags. For example, we use January SSTs in conjunction with the Little Colorado's January–March precipitation to obtain Pearson's correlation coefficients at each grid cell in the oceanic domain. Pearson's product moment correlation coefficients take the form

$$r = \frac{\sum_{i=1}^{n}(x_i - \overline{x})(y_i - \overline{y})}{(n-1)s_x s_y}, \tag{1}$$

where x_i and y_i are individual measurements in the sample size n, $\overline{x}$ and $\overline{y}$ are the sample means of $\mathbf{x}$ and $\mathbf{y}$ with standard deviations of s_x and s_y. The correlation coefficients range from −1 to 1, where the two variables are most well correlated when closest to −1 and 1, with 0 having no correlation. Pearson's correlation coefficients are commonly used with Gaussian distributed data. The correlation map that is created is identified by JAN-PL1 (where JAN corresponds to January SSTs, P is precipitation and L1 is the lag of the middle month of the seasonal precipitation with respect to the SST month). The temporal correlative structure is observed next. Correlation maps are created for the other 11 seasons, at different temporal lags behind January SSTs. Now we have maps corresponding to JAN-PL2 through JAN-PL12. The procedure is repeated for the other 11 months of SSTs as our predictors. Seasonal basin precipitation corresponds to 144 correlation maps (12 SST months × 12 seasonal lags). The same procedure is performed for the Little Colorado's temperature and discharge, which provides 144 correlation maps for each of these variables (432 maps total). The map

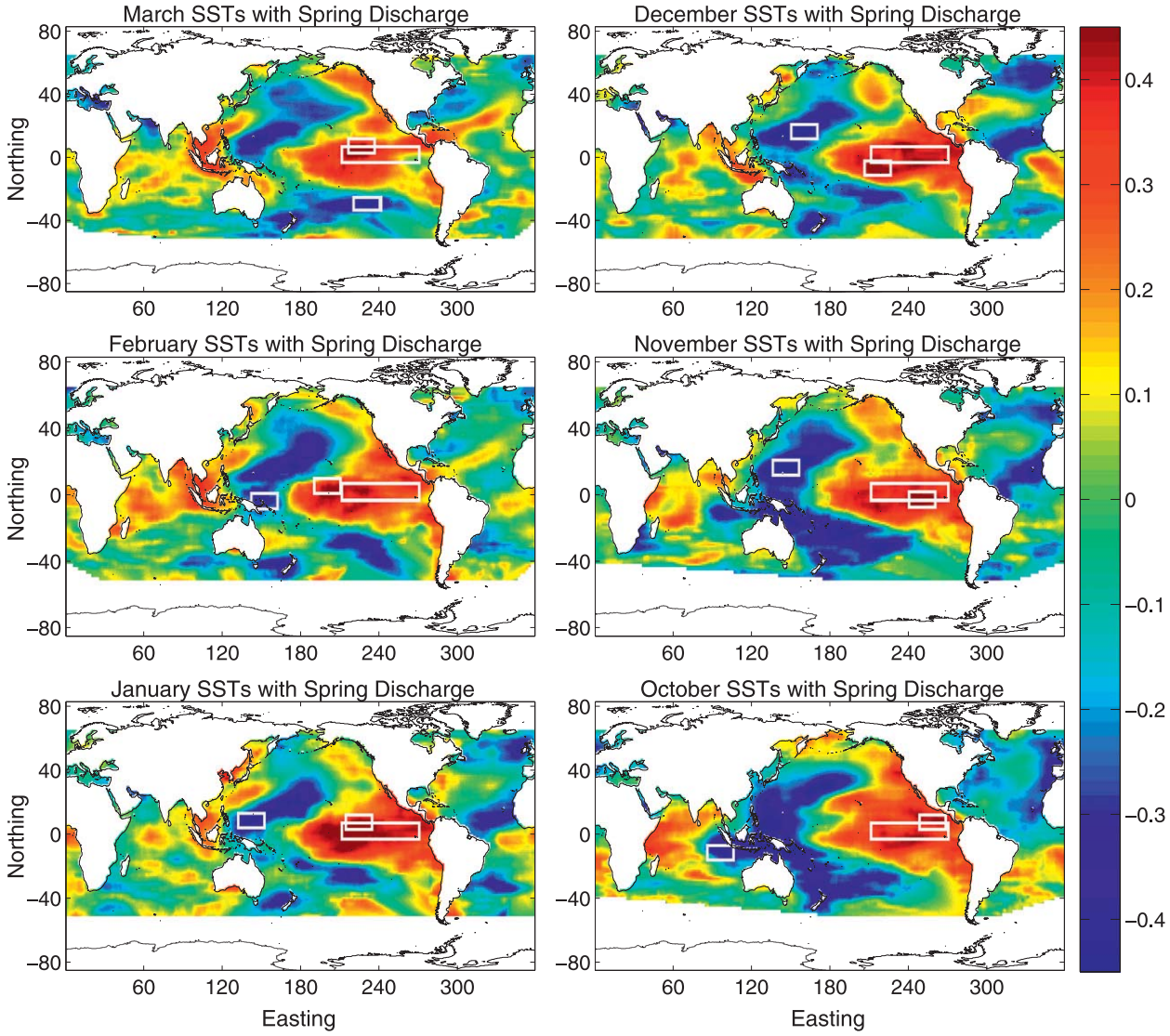

FIG. 2. Little Colorado's structure of correlation coefficients for SST months and March–May (spring) discharge at increasing lag times. The smaller rectangles correspond to the most positively and negatively correlated regions, while the larger rectangle is that of the Niño-3 domain.

identification follows the same structure—for example, FEB-TL1 and MAY-DL9 (where T is temperature and D is discharge). The entire process is then repeated using the Gunnison's unique seasonal hydroclimatic time series.

Figures 2 and 3 show examples of the progression of the oceanic correlative structures for the Little Colorado and Gunnison, respectively. One can observe the robustness of these structures, by the consistency of the patterns, when spring discharge is correlated with increasingly earlier monthly SSTs. The most correlated windows for the Little Colorado are predominantly located around the equatorial Pacific. The Gunnison, however, has a consistent correlation structure in the North Pacific. As a result, one expects for these cases that the ENSO indices and the PDO will be well correlated with the Little Colorado and Gunnison, respectively.

b. Regions of high correlation

Using the correlation coefficients, the most positively and negatively correlated windows (the 10° × 20° latitude by longitude SST windows) across the globe are identified for all combinations of months, lags, and basin variables. Most likely, a different window will correspond to each combination (although different combinations do not necessitate a different window, they could overlap, or be identical in space). Next, the larger of the two most correlated windows, by absolute magnitude, is used to extract the most predictive power from the

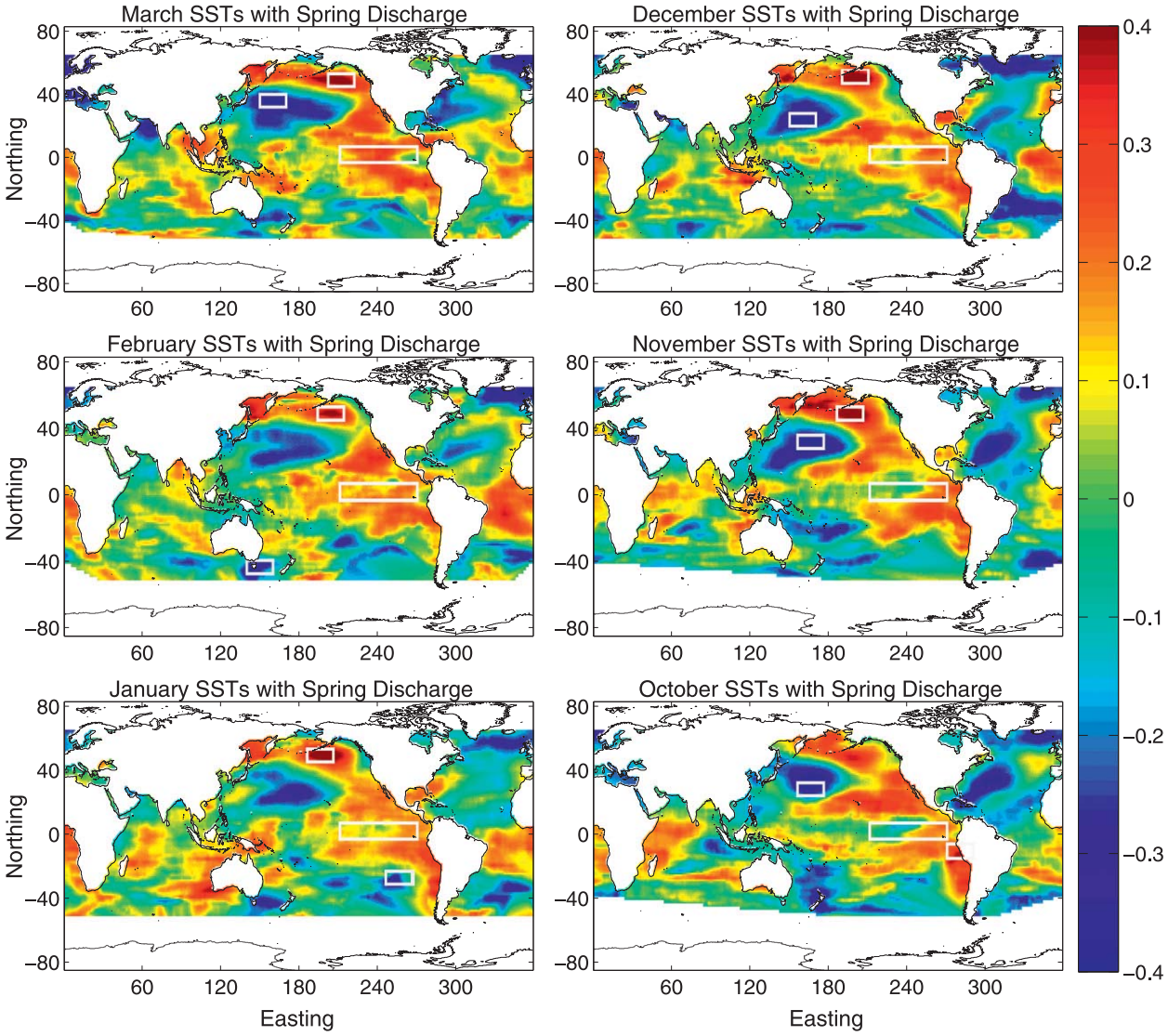

FIG. 3. Same as Fig. 2 but for Gunnison.

corresponding SSTs. There are now 432 SST windows that can be used to quantitatively predict the seasonal hydroclimates in the Little Colorado and Gunnison—as much as a year in advance.

How do the magnitudes of the correlation coefficients change through the year at different lags for both basins? Figures 4 and 5 contrast the correlative magnitude using BSCP (the most correlated SSTs) to Niño-3, Niño-3.4, MEI, and PDO for the Little Colorado and Gunnison, respectively. Using only SSTs as our predictors, at regions that we allow to vary in space, we find stronger correlations than when using the other four standard climate indices as predictors. As mentioned in the previous section, the ENSO indices have a fairly strong correlation with spring discharge in the Little Colorado. However, Gunnison's spring discharge is only significantly correlated with the PDO at lag 1. The statistical correlation using the standard indices is further reduced for almost all other seasons and lags. In the Little Colorado, there are only two instances when one of the standard indices is more strongly correlated than BSCP. The MEI has correlation coefficients of 0.57 for OCT-PL5 and 0.49 for FEB-DL2, whereas BSCP has 0.56 and 0.46, respectively. The BSCP observes stronger correlation for all cases in the Gunnison.

c. *Assessing uncertainty*

An efficient way to assess the uncertainty associated with individual predictions is by using a mixture of Gaussians (McLachlan and Peel 2000; Wójcik et al.

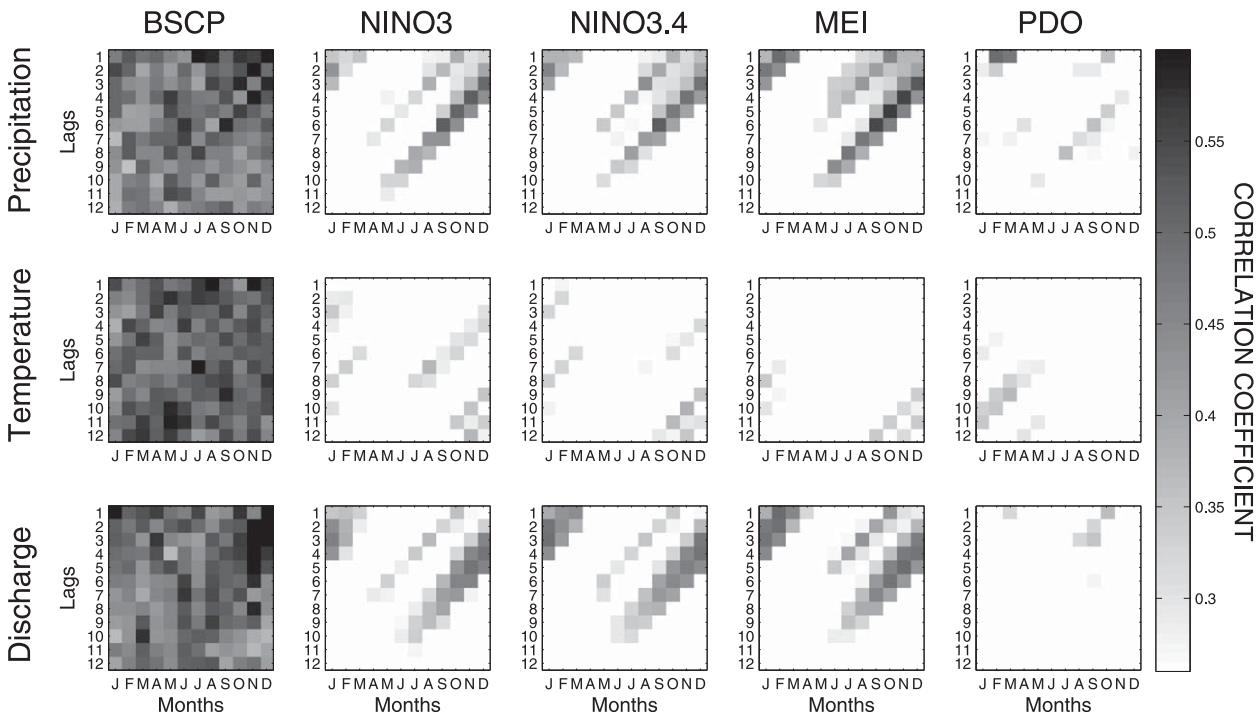

FIG. 4. Absolute magnitude of the correlation coefficients for the Little Colorado through the year and at different lags for the hydroclimatic variables using BSCP vs the standard climate indices. The lower limit of the colorbar is 0.27, which is statistically significant at the 95% confidence level.

2006). Gaussian mixture models (GMMs) form clusters by representing the probability density function (PDF) of observed variables as a mixture of multivariate Gaussian densities. The distribution is fit to the data using an expectation maximization (EM) algorithm (McLachlan and Peel 2000), which assigns joint probabilities across x and y space in the case of a two-dimensional scatterplot. GMMs are most appropriate to use when it is obvious that there is more than one distinct region where the data have gravitated—for example, there is bimodality in the aggregation of the scatter. In our analysis, we did not observe more than one distinct cluster for the hydroclimatic data in the Little Colorado and Gunnison. Hence, a GMM with one cluster is used. It should be made clear that the GMM's results with one cluster are the same as would be obtained with a linear regression. Our methodology, however, uses GMMs instead of linear regression, to be more broadly applicable to basins that could have data exhibiting nonlinearity.

The strength of the GMM regression by itself does not say much about the predictive/hindcast skill. Therefore, a series of Monte Carlo simulations are performed as a robust measure to assess the model's skill. Figure 6 provides an example of one of the simulations using the GMM. The data in Fig. 6 corresponds to the positively correlated window's December SST time series and the Gunnison's spring discharge (upper-right plot in Fig. 3). This scatter has a correlation coefficient of 0.54. The bold circles in Fig. 6a, which constitute 30 randomly chosen points from the scatter, are used to predict the other lighter circles. These 30 points are used to obtain the GMM (Fig. 6b). Next, a slice of the GMM is taken at the December SST z score of one of the lighter circles (surrounded by the larger circle in Fig. 6a). Normalizing this slice gives the PDF and the cumulative distribution function (CDF) of March–May discharge (Figs. 6c and 6d, respectively). The highest peak on the PDF is the most probable discharge, whereas the corresponding CDF is used to assess the 5% and 95% nonexceedence discharges. Similarly, PDFs and CDFs are obtained for all other lighter circles. These hindcasts of the lighter circles are stored, and the points are reshuffled to yield another random 30 bold circles to predict a new set of lighter circles. One hundred different simulations are performed. All of the stored values at each point are then used to obtain average quantities of the most probable 5% and 95% nonexceedence discharges. Lastly, the normally distributed data is converted back to a gamma distribution. This approach of using GMM regression with Monte Carlo simulations was also used to perform the hindcasts with the different climate indices' time series as predictors.

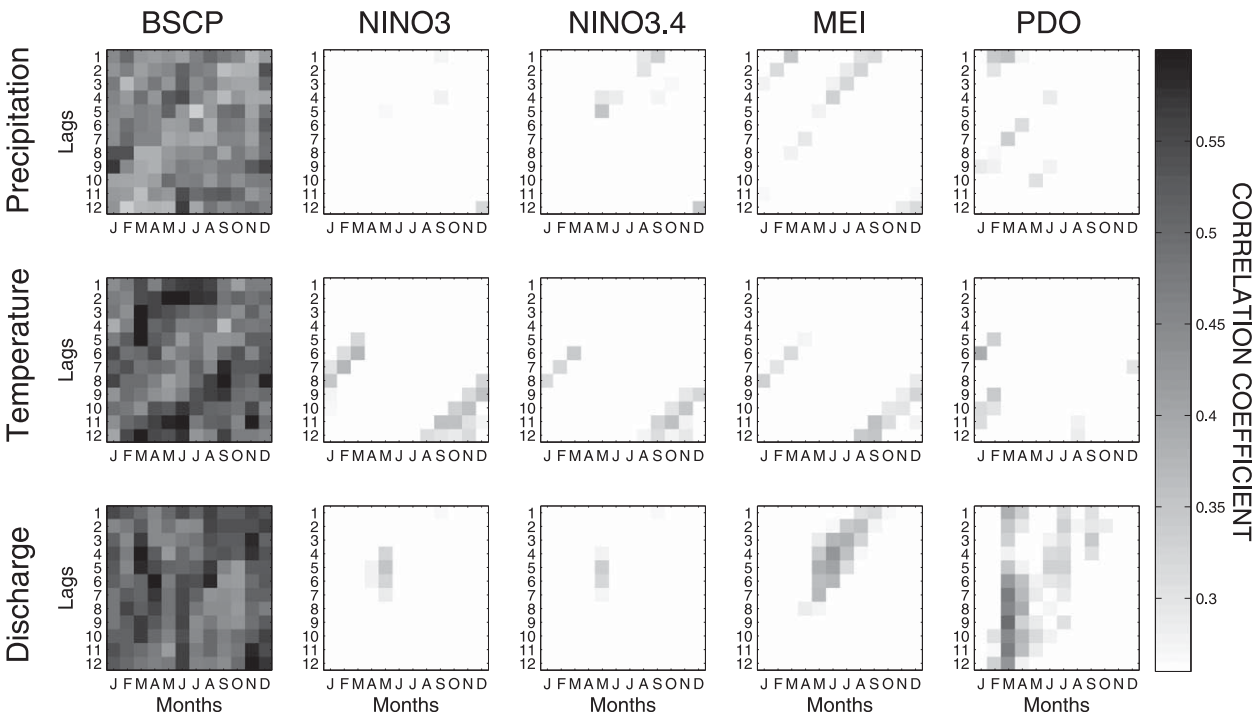

FIG. 5. Same as Fig. 4 but for Gunnison.

Figure 7 shows the hindcasts of the March–May discharge volume (average depth of water over the Gunnison basin) given December SSTs. The dark line shows the observed discharge, whereas the light gray line going through the middle is the observed mean discharge. The circles are the most probable hindcasts, whereas the error bars correspond to the 5% and 95% nonexceedence values. The skill of these hindcasts in contrast to the standard climate indices and the historic hydroclimatology is addressed in the next section.

4. Results

Two parameters are used to assess the predictive skill of each set of hindcasts. The parameters are model correlation coefficient and the Nash–Sutcliffe efficiency (NSE). The model correlation coefficient is calculated with Eq. (1) using modeled versus observed data. NSE is defined as

$$\mathrm{NSE} = 1 - \frac{\sum_{t=1}^{T} (x_o^t - x_m^t)^2}{\sum_{t=1}^{T} (x_o^t - \overline{x}_o)^2}, \qquad (2)$$

where $\overline{x}_o$ is the mean of observed values and x_o^t and x_m^t are the observed and modeled values at time t, respectively. The NSE has historically been used to assess the skill that a hydrologic model has in matching observed hydrographs. It is used here, more generally, to assess the hindcast skill in contrast to simply using the hydroclimatic means of discharge, precipitation, and temperature. NSE ranges from negative infinity to one. A value of one is for perfect hindcasts, whereas values greater than zero indicate when the model is performing better, or hindcasting better, than the hydroclimatic mean. Conversely, values fewer than zero delineate instances when the hydroclimatic mean would give better results than the model.

Figure 8 shows the model's performance, for the Little Colorado, expressed as correlation coefficients that are obtained from observed versus modeled hydroclimate values. With darker shading, the model is more skillfully hindcasting. Figure 9 uses the NSE to give a perspective into how well the hindcasts are doing in contrast to the Little Colorado's hydroclimatic mean. Figures 10 and 11 similarly show the correlation coefficients (observed versus modeled) and NSE values for the Gunnison, respectively. Moderate hindcast skill is observed in both basins, using BSCP, for winter precipitation and temperature throughout the year at a variety of lags. BSCP also hindcasts discharge better in both basins than using the standard indices, though there is substantial difference in skill between the Little Colorado and the Gunnison. The discharge hindcasts using BSCP are much better for the Gunnison. Possible explanations as to why we observe significant differences in the basins' discharge hindcasts is discussed in the following section.

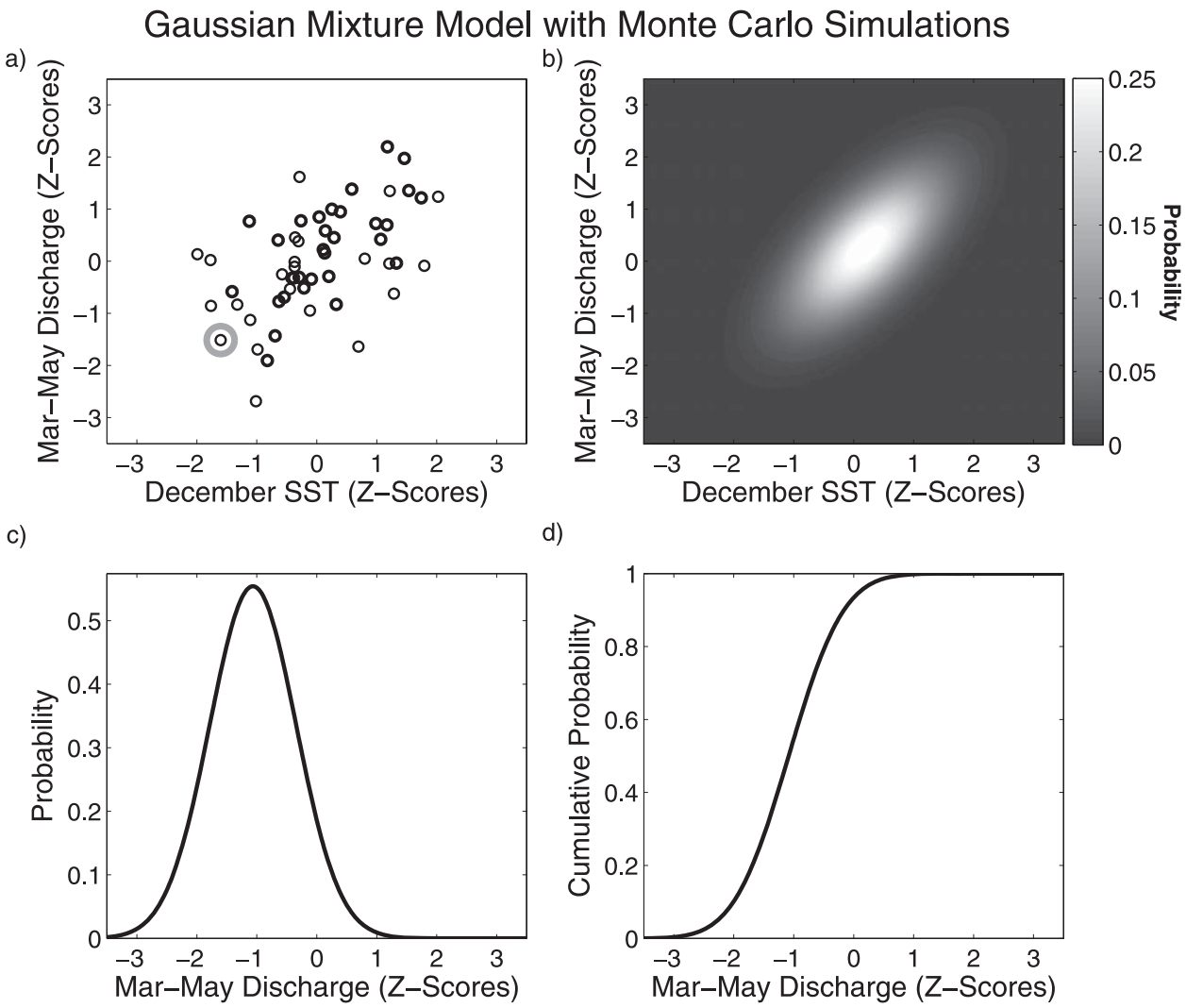

FIG. 6. Applying the GMM with Monte Carlo simulations: (a) the scatter of December SSTs and Gunnison's March–May discharge, where the more bold points are used to hindcast the lighter points; the lighter point that is circled will be the first point to be hindcasted; (b) the resulting GMM; (c) the PDF that corresponds to the slice along the SST z score of the point that is circled; and (d) CDF of the same slice.

5. Discussion and conclusions

This paper has explored the unique statistical relationships that relate global SSTs with the Little Colorado and Gunnison basins' hydroclimates. The advantage of BSCP is that it targets an oceanic region that maximizes the correlation for a specific basin at a given time. As a result, improvement in hydroclimatic seasonal hindcasts has been shown over the standard climate indices.

The work presented here raises several issues that require further analysis and can be improved in three ways. First, the weak-to-moderate skill observed for the Little Colorado's discharge requires improvement. This is the result of the basin's antecedent conditions upon entering the hindcast/forecast season [e.g., soil moisture and snow water equivalent (SWE)]. A basin's storage acts as a nonlinear filter for discharge in response to precipitation and temperature forcings (Troch et al. 2007). During the seasons with significant snowmelt, the Gunnison receives on average approximately 4 times the amount of precipitation than the Little Colorado. Additionally, the Gunnison's temperatures are substantially lower than in the Little Colorado. These conditions create a likely scenario for the Little Colorado's snowpack to quickly melt and subsequently dry out the soil. On the other hand, the Gunnison's soil rarely becomes depleted of moisture. These fluctuations in the Little Colorado's soil moisture have a significant effect on its discharge,

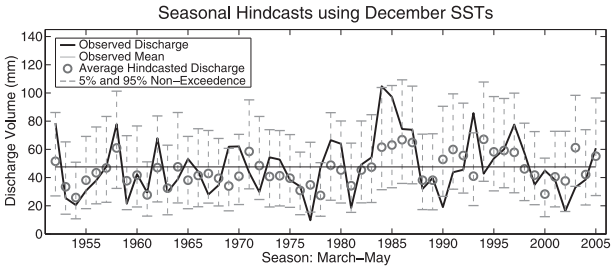

FIG. 7. Hindcasts of Gunnison's March–May total discharge volume using December SSTs.

ultimately reducing the observed hindcast skill level. A hydrological model can better capture the physical processes of precipitation and temperature interacting with differing ranges of soil moisture and SWE to produce a given discharge. Therefore, a hydrological model could be forced with precipitation and temperature hindcasts/forecasts from the BSCP model to produce physically viable realizations of discharge. Seasonal forecasts of basin discharges, which are significantly affected by SWE, can also be updated throughout the winter and early spring as new SWE data becomes available. Second, the predictors (SSTs) can be supplemented with additional oceanic or atmospheric variables (e.g., sea level pressures, wind vectors, geopotential heights). The current scope of this work provides a methodology that obtains the most correlated SST regions and essentially uses a linear regression for hindcasting. This alone has shown potential skill in forecasting. However, rooting the predictors in multiple variables can improve forecast skill by increasing the robustness of the methodology. Furthermore, using an objective combination of a variety of statistical methods [e.g., PCA, screening multiple linear regression (SMLR), optimal climate normals (OCN) or some other trend detection] on a set of time series obtained from multiple variables using BSCP can further increase hindcast/forecast skill similarly to the CPC (O'Lenic et al. 2008). Lastly, the nonstationarity of the correlative statistical patterns requires consideration (Milly et al. 2008). Though adding one additional scatter point will change the correlation in a given location (in most cases), this is a relatively slow process. With the inclusion of an additional year of data, the correlation maps will not be drastically altered. However, the locations of strongest correlation will shift over time because of system dynamics and trending. Both SSTs and land surface temperatures appear to be exhibiting trending (Moron et al. 1998; Jones et al. 1999; Stott et al. 2000). If we are going to successfully translate the BSCP methodology from hindcasting to forecasting, then the nonstationarity exhibited by the ocean–atmosphere–land system must be accounted for in the process. Additionally, to better

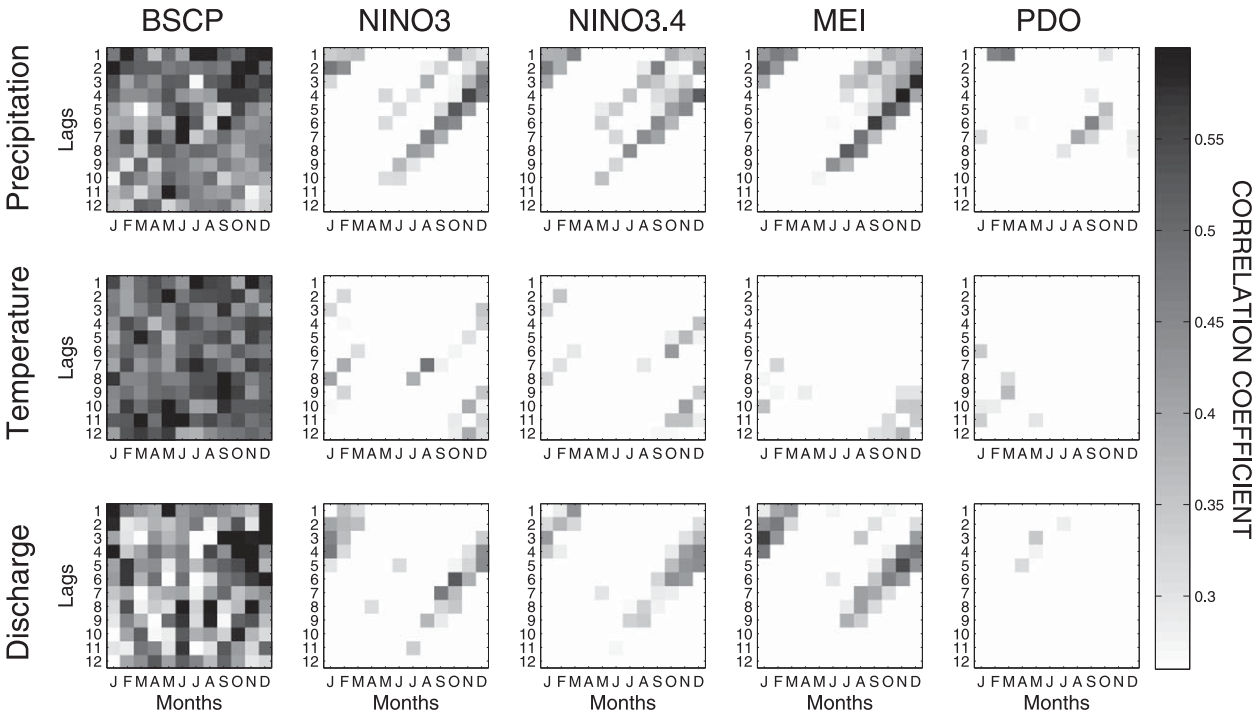

FIG. 8. Little Colorado's correlation coefficients for the hindcasts vs observed hydroclimatic values.

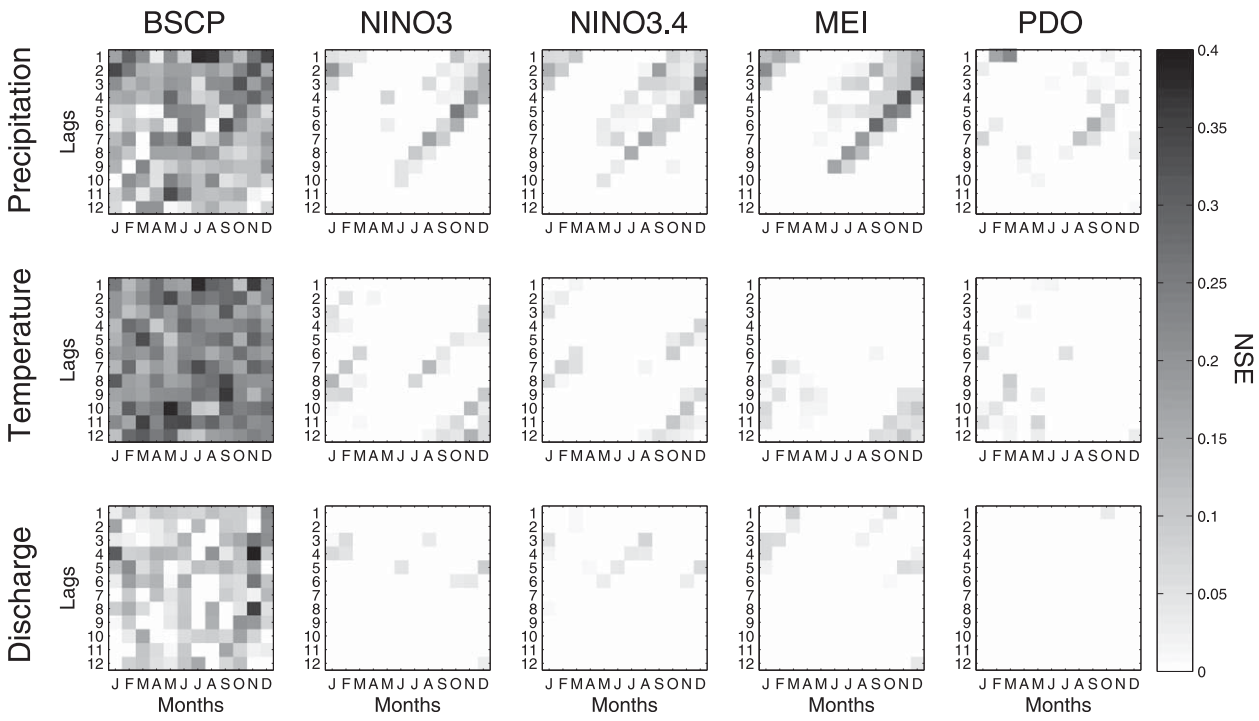

FIG. 9. NSE for the Little Colorado. The darker the shading, the more skillful the hindcasts are in comparison to the hydroclimatic mean.

observe the evolution of these patterns, given trending, it would be advantageous to drop or less heavily weight older data. For example, the last 30–40 years of data (updated each year, adding an additional year, and dropping the last one) can be used to forecast next year's hydroclimate.

Applying BSCP across a multitude of basins, in varying climate regions, has the potential to improve seasonal

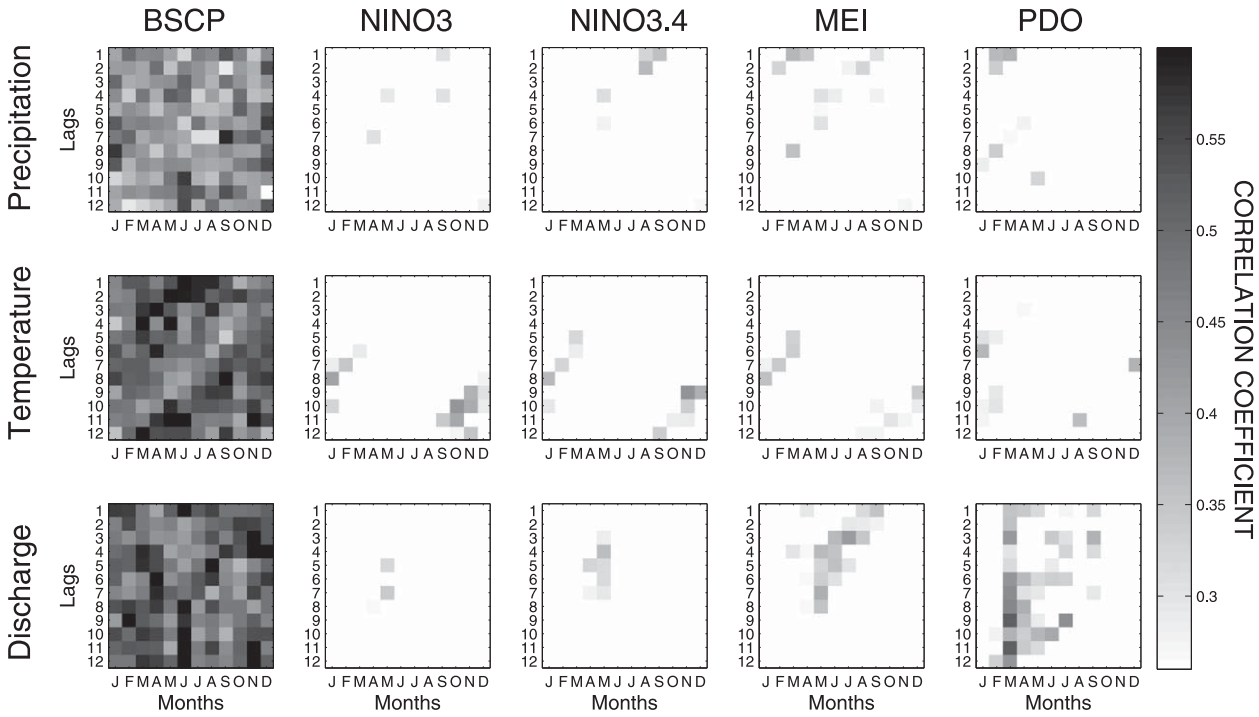

FIG. 10. Same as Fig. 8 but for Gunnison.

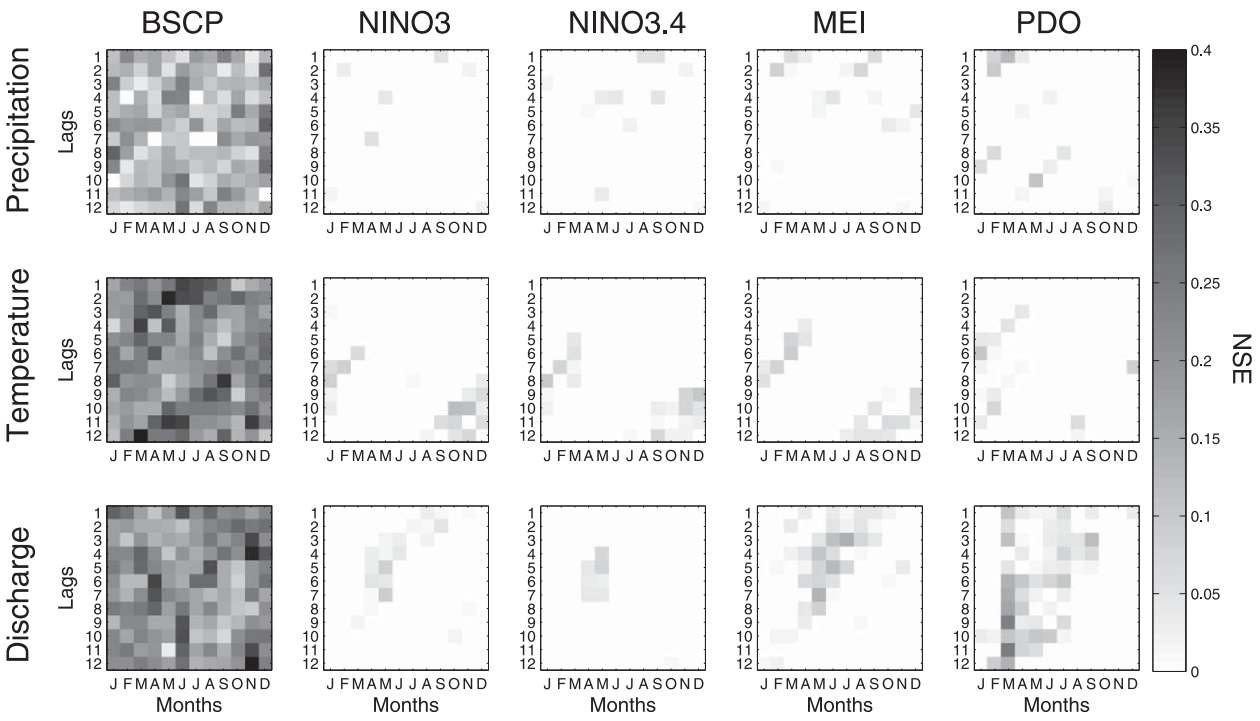

FIG. 11. Same as Fig. 9 but for Gunnison.

hydroclimatic predictions across the globe. Ultimately, we want to know the dynamical interactions that govern the observed statistical patterns. We are currently observing how these spatiotemporal statistical patterns shift between basins, though this is a work in progress. The cross-basin statistical relationships that arise could assist in formulating a new physical understanding of ocean–atmosphere–land interactions. If attained, improved understanding of the causes of seasonal hydroclimatic variability will greatly benefit water resources management.

Acknowledgments. The authors thank the Bureau of Reclamation, Lower Colorado Regional Office, for funding this study. Terry Fulp and Kathy Jacobs have offered invaluable advice and support. We wish to acknowledge Dennis Lettenmaier and Edwin Maurer for the use of Maurer's dataset. Useful discussions with Matej Durcik, Maite Guardiola-Claramont, and Seshadri Rajagopal are very much appreciated.

REFERENCES

Abramovitz, M., and I. A. Stegun, 1972: *Handbook of Mathematical Functions*. 9th ed. Dover, 1046 pp.

Barnett, T. P., J. C. Adam, and D. P. Lettenmaier, 2005: Potential impacts of a warming climate on water availability in snow-dominated regions. *Nature,* **438,** 303–309.

——, and Coauthors, 2008: Human-induced changes in the hydrology of the western United States. *Science,* **319,** 1080–1083.

Cayan, D. R., K. T. Redmond, and L. G. Riddle, 1999: ENSO and hydrologic extremes in the western United States. *J. Climate,* **12,** 2881–2893.

Christensen, N. S., and D. P. Lettenmaier, 2007: A multimodel ensemble approach to climate change impacts on the hydrology and water resources of the Colorado River Basin. *Hydrol. Earth Syst. Sci.,* **11,** 1417–1434.

——, A. W. Wood, N. Voisin, D. P. Lettenmaier, and R. N. Palmer, 2004: Effects of climate change on the hydrology and water resources of the Colorado basin. *Climatic Change,* **62,** 337–363.

Dettinger, M. D., and D. R. Cayan, 1995: Large-scale atmospheric forcing of recent trends toward early snowmelt runoff in California. *J. Climate,* **8,** 606–623.

Enfield, D. B., A. M. Mestas-Nuñez, and P. J. Trimble, 2001: The Atlantic multidecadal oscillation and its relation to rainfall and river flows in the continental U.S. *Geophys. Res. Lett.,* **28,** 2077–2080.

Gochis, D. J., L. Brito-Castillo, and W. J. Shuttleworth, 2007: Correlations between sea-surface temperatures and warm season streamflow in northwest mexico. *Int. J. Climatol.,* **27,** 883–901.

Grantz, K., B. Rajagopalan, M. Clark, and E. Zagona, 2005: A technique for incorporating large-scale climate information in basin-scale ensemble streamflow forecasts. *Water Resour. Res.,* **41,** W10410, doi:10.1029/2004WR003467.

Higgins, R. W., Y. X. Leetmaa, and A. Barnston, 2000: Dominant factors influencing the seasonal predictability of U.S. precipitation and surface air temperature. *J. Climate,* **13,** 3994–4017.

Hoerling, M., and J. Eischeid, 2007: Past peak water in the Southwest. *Southwest Hydrol.,* **6,** 18–19.

Jones, P. D., M. New, D. E. Parker, S. Martin, and I. G. Rigor, 1999: Surface air temperature and its changes over the past 150 years. *Rev. Geophys.,* **32,** 173–199.

Kim, T. W., J. B. Valdés, B. Nijssen, and D. Roncayolo, 2005: Quantification of linkages between large-scale climatic patterns and precipitation in the Colorado River Basin. *J. Hydrol.,* **321,** 173–186.

Kutzbach, J. E., 1970: Large-scale features of monthly mean Northern Hemisphere anomaly maps of sea-level pressure. *Mon. Wea. Rev.,* **98,** 708–716.

Mantua, N. J., S. R. Hare, Y. Zhang, J. M. Wallace, and R. C. Francis, 1997: A Pacific interdecadal climate oscillation with impacts on salmon production. *Bull. Amer. Meteor. Soc.,* **78,** 1069–1079.

Maurer, E. P., A. W. Wood, J. C. Adam, D. P. Lettenmaier, and B. Nijssen, 2002: A long-term hydrologically based dataset of land surface fluxes and states for the conterminous United States. *J. Climate,* **15,** 3237–3251.

McCabe, G. J., and M. D. Dettinger, 1999: Decadal variations in the strength of ENSO teleconnections with precipitation in the western United States. *Int. J. Climatol.,* **19,** 1399–1410.

——, and D. M. Wolock, 2007: Warming may create substantial water supply shortages in the Colorado River basin. *Geophys. Res. Lett.,* **34,** L22708, doi:10.1029/2007GL031764.

McKee, T. B., N. J. Doesken, and J. Kleist, 1993: The relationship of drought frequency and duration to time scales. Preprints, *Eighth Conf. on Applied Climatology,* Anaheim, CA, Amer. Meteor. Soc., 179–184.

McLachlan, G., and D. Peel, 2000: *Finite Mixture Models*. John Wiley & Sons, 419 pp.

Milly, P. C. D., K. A. Dunne, and A. V. Vecchia, 2005: Global pattern of trends in streamflow and water availability in a changing climate. *Nature,* **438,** 347–350.

——, J. Betancourt, M. Falkenmark, R. M. Hirsch, Z. W. Kundzewicz, D. P. Lettenmaier, and R. J. Stouffer, 2008: Stationarity is dead: Whither water management? *Science,* **319,** 573–574.

Moron, V., R. Vautard, and M. Ghil, 1998: Trends, interdecadal and interannual oscillations in global sea-surface temperatures. *Climate Dyn.,* **14,** 545–569.

Namias, J., 1969: Seasonal interactions between North Pacific Ocean and the atmosphere during the 1960's. *Mon. Wea. Rev.,* **97,** 173–192.

——, 1974: Longevity of a coupled air–sea–continent system. *Mon. Wea. Rev.,* **102,** 638–648.

——, 1978: Multiple causes of the North American abnormal winter 1976–1977. *Mon. Wea. Rev.,* **106,** 279–295.

——, and D. R. Cayan, 1984: El Niño: Implications for forecasting. *Oceanus,* **27,** 41–47.

Nicholls, N., 1980: Long-range weather forecasting: Value, status, and prospects. *Rev. Geophys.,* **18,** 771–788.

O'Lenic, E. A., D. A. Unger, M. S. Halpert, and K. S. Pelman, 2008: Developments in operational long-range climate prediction at CPC. *Wea. Forecasting,* **23,** 496–515.

Piechota, T. C., J. A. Dracup, and R. G. Fovell, 1997: Western US streamflow and atmospheric circulation patterns during El Niño-Southern Oscillation. *J. Hydrol.,* **201,** 249–271.

Redmond, K. T., and R. W. Koch, 1991: Surface climate and streamflow variability in the western United States and their relationship to large-scale circulation indices. *Water Resour. Res.,* **27,** 2381–2399.

Ropelewski, C. F., and M. S. Halpert, 1996: Quantifying Southern Oscillation precipitation relationships. *J. Climate,* **9,** 1043–1059.

Rucong, Y., Z. Minghua, Y. Yongqiang, and L. Yimin, 2001: Summer monsoon rainfalls over mid-eastern China lagged correlated with global SSTs. *Adv. Atmos. Sci.,* **18,** 179–196.

Stott, P. A., S. F. Tett, G. S. Jones, M. R. Allen, J. F. Mitchell, and G. J. Jenkins, 2000: External control of 20th century temperature by natural and anthropogenic forcings. *Science,* **290,** 2133–2137.

Tootle, G. A., and T. C. Piechota, 2006: Relationships between Pacific and Atlantic ocean sea surface temperatures and U.S. streamflow variability. *Water Resour. Res.,* **42,** W07411, doi:10.1029/2005WR004184.

Trenberth, K. E., 1997: The definition of El Niño. *Bull. Amer. Meteor. Soc.,* **78,** 2771–2777.

Troch, P. A., M. Durcik, S. Seneviratne, M. Hirschi, A. Tueling, R. Hurkmans, and S. Hasan, 2007: New data sets to estimate terrestrial water storage change. *Eos, Trans. Amer. Geophys. Union,* **88,** doi:10.1029/2007EO450001.

Wójcik, R., P. A. Troch, H. Stricker, P. Torfs, E. Wood, H. Su, and Z. Su, 2006: Mixtures of Gaussians for uncertainty description in bivariate latent heat flux proxies. *J. Hydrometeor.,* **7,** 330–345.